









Origins and effects of mix on magnetized liner inertial fusion target performance

Cite as: Phys. Plasmas **26**, 012704 (2019); <https://doi.org/10.1063/1.5064548>

Submitted: 05 October 2018 . Accepted: 21 December 2018 . Published Online: 11 January 2019

P. F. Knapp , M. R. Gomez , S. B. Hansen, M. E. Glinsky, C. A. Jennings, S. A. Slutz , E. C. Harding, K. D. Hahn, M. R. Weis , M. Evans, M. R. Martin, A. J. Harvey-Thompson, M. Geissel , I. C. Smith, D. E. Ruiz , K. J. Peterson , B. M. Jones, J. Schwarz, G. A. Rochau, D. B. Sinars, R. D. McBride, and P.-A. Gourdain 



View Online



Export Citation



CrossMark

ARTICLES YOU MAY BE INTERESTED IN

[Enhancing performance of magnetized liner inertial fusion at the Z facility](#)

Physics of Plasmas **25**, 112706 (2018); <https://doi.org/10.1063/1.5054317>

[Alpha heating enhancement in MagLIF targets: A simple analytic model](#)

Physics of Plasmas **26**, 012705 (2019); <https://doi.org/10.1063/1.5079519>

[Diagnosing and mitigating laser preheat induced mix in MagLIF](#)

Physics of Plasmas **25**, 112705 (2018); <https://doi.org/10.1063/1.5050931>



ULVAC

Leading the World with Vacuum Technology

- Vacuum Pumps
- Arc Plasma Deposition
- RGAs
- Leak Detectors
- Thermal Analysis
- Ellipsometers

Origins and effects of mix on magnetized liner inertial fusion target performance

Cite as: Phys. Plasmas **26**, 012704 (2019); doi: [10.1063/1.5064548](https://doi.org/10.1063/1.5064548)

Submitted: 05 October 2018 · Accepted: 21 December 2018 · Published Online:

11 January 2019



P. F. Knapp,¹ M. R. Gomez,¹ S. B. Hansen,¹ M. E. Glinsky,¹ C. A. Jennings,¹ S. A. Slutz,¹ E. C. Harding,¹ K. D. Hahn,^{1,a)} M. R. Weis,¹ M. Evans,² M. R. Martin,¹ A. J. Harvey-Thompson,¹ M. Geissel,¹ I. C. Smith,¹ D. E. Ruiz,¹ K. J. Peterson,¹ B. M. Jones,¹ J. Schwarz,¹ G. A. Rochau,¹ D. B. Sinars,¹ R. D. McBride,² and P.-A. Gourdain³

AFFILIATIONS

¹ Sandia National Laboratories, Albuquerque, New Mexico 87185, USA

² Department of Nuclear Engineering and Radiological Sciences, University of Michigan, Ann Arbor, Michigan 48109, USA

³ Department of Physics and Astronomy, University of Rochester, Rochester, New York 14627, USA

^{a)} Current Address: Lawrence Livermore National Laboratory, Livermore, California 94550.

ABSTRACT

In magneto-inertial-fusion experiments, energy losses such as a radiation need to be well controlled in order to maximize the compressional work done on the fuel and achieve thermonuclear conditions. One possible cause for high radiation losses is high-Z material mixing from the target components into the fuel. In this work, we analyze the effects of mix on target performance in Magnetized Liner Inertial Fusion (MagLIF) experiments at Sandia National Laboratories. Our results show that mix is likely produced from a variety of sources, approximately half of which originates during the laser heating phase and the remainder near stagnation, likely from the liner deceleration. By changing the “cushion” component of MagLIF targets from Al to Be, we achieved a $10\times$ increase in neutron yield, a 60% increase in ion temperature, and an $\sim 50\%$ increase in fuel energy at stagnation.

Published under license by AIP Publishing. <https://doi.org/10.1063/1.5064548>

I. INTRODUCTION

The Magnetized Liner Inertial Fusion (MagLIF) concept is an approach to inertial confinement fusion which uses a cylindrical implosion with a pre-imposed axial magnetic field ($B_{z,0}$), which inhibits thermal conduction and traps fusion products, and laser heated fusion fuel to reduce the driver power and fuel areal density (ρR) required to achieve self-heating of fusion fuel.¹ Initial experimental results have demonstrated significant thermonuclear fusion yield [$\geq 10^{12}$ deuterium-deuterium (DD) neutrons]^{2,3} and fuel magnetization at stagnation,^{4,5} proving the viability of this approach and the efficacy of laser preheating and pre-magnetization in achieving thermonuclear conditions. Despite these promising results, key stagnation parameters (e.g., ion temperature T_i , neutron yield Y_{DD} , and stagnation pressure P_{stag}) are below predictions.⁶ One hypothesis for reduced target performance is that material mixing from the target components into the fuel causes higher radiation losses. In this paper, we specifically study the impact of mix on the performance of MagLIF experiments. We infer an effective total mix fraction for two different classes of experiments and analyze the contributions from various sources of mix. We show that mix introduced

into the target at the time of laser heating has a dramatic negative effect on yield and stagnation pressure, while mix introduced at or near stagnation is significantly less detrimental.

In these experiments, a Be cylinder holding 60 PSI of pure deuterium (D_2) gas, shown in Fig. 1(a), is preheated using the multi-kJ Z-Beamlet (ZBL) laser^{7,8} and imploded in ≈ 100 ns using the 20 MA Z machine at Sandia National Laboratories.⁹ Figure 1(b) shows a cross-section of the load region with the field coils used to provide the 10 T initial field oriented along the axis of the cylinder with a rise time of ≈ 3 ms.¹⁰ The ZBL laser enters the target from above. The beam is $f/10$ and is unsmoothed in these experiments. The effects of beam conditioning on mix and energy deposition are reported elsewhere.^{3,11} The focus of the beam is offset such that the beam spot is ~ 500 μm on the window with an approximately square shape. In the laser heating configuration used here, we employ a pre pulse and a main pulse, separated by ≈ 3 ns. The purpose of the pre pulse is to ionize and expand the window to allow sufficient transmission of the main pulse into the fuel. The current pulse, along with the ZBL laser monitor signal, and x-ray pulse produced at stagnation are shown in Fig. 1(c). A sample liner trajectory from a 1D

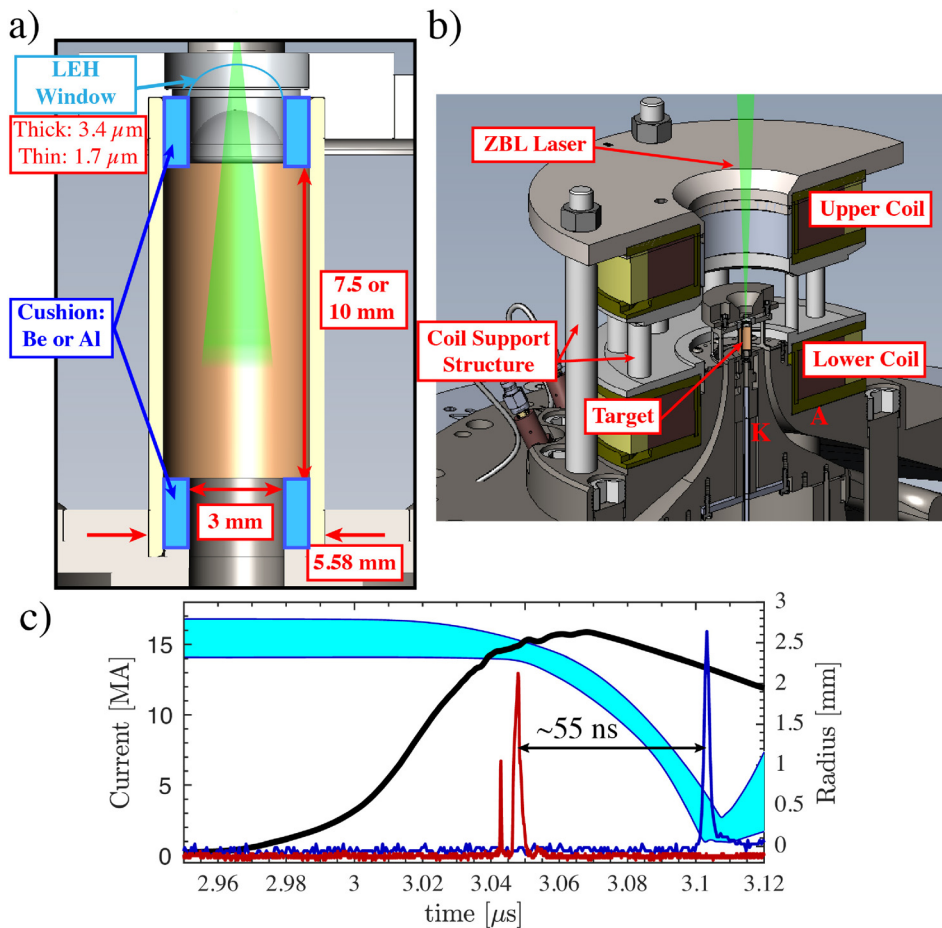


FIG. 1. (a) Illustration of the MagLIF target used in this study. Experiments were performed with Be and Al cushions, highlighted in blue. (b) A typical MagLIF experiment showing the final power feed (labeled “A” and “K” for the anode and cathode), target, laser beam, and the field coils. (c) Overview of the evolution of a MagLIF target. Current delivered to the load (black), 1D liner trajectory (cyan filled curve), laser monitor signal (red), and x-rays produced at stagnation (blue). The dwell time between laser heating and stagnation is ~ 55 ns.

calculation^{12,13} is shown as the cyan curve. In these experiments, the time delay between laser heating and stagnation is 55 ns. This relatively long dwell time makes the targets particularly sensitive to mix generated during the laser heating phase.

Figure 2(a) shows the neutron yield as a function of ion temperature for a wide range of experiments. The ion temperature is derived from the width of the neutron spectrum, measured using neutron time of flight detectors.¹⁴ There is a clear trend showing increasing yield with ion temperature in a manner which is consistent with the DD fusion reactivity. Figure 2(b) shows the same experiments; however, this time, the ratio of the x-ray to neutron yield, Y_x/Y_{DD} , is plotted as a function of ion temperature. Based on the relation between mix and radiation losses, Y_x/Y_{DD} can serve as a metric for quantifying material mix into the fuel,¹⁵ and indeed, experiments with lower temperatures and correspondingly lower neutron yield show a higher value of Y_x/Y_{DD} . The two clusters of points highlighted in cyan and magenta are the focus of this study. In the experiments represented by the cyan points, the metal cushions, highlighted in blue in Fig. 1(a) at the top and bottom of the target, were made of Al, while they were made of Be in the experiments represented by the magenta points. These experiments were otherwise identical, employing nominally identical laser pulses, gas fills, window thickness, and target

dimensions. The metal cushions are required to mitigate the so-called wall instability and prevent the top and bottom portions of the liner from imploding prematurely.¹⁶ The target parameters and performance of each of these experiments are summarized in Table I. The Be cushion targets have $\sim 10\times$ higher neutron yield and $\sim 60\%$ higher ion temperature. The x-ray to neutron yield ratio for the Be targets is $\sim 3\text{--}5\times$ smaller than the Al cushion targets, all of which suggests that mix from the cushions generated during laser heating is strongly affecting the performance in these experiments. This result was entirely unexpected, as detailed 2D simulations did not predict any significant mix originating from the cushion or the Laser Entrance Hole (LEH) window.

The remainder of this paper is organized as follows: In Sec. II, we analyze the data from two groups of experiments to determine the stagnation pressure and effective mix fraction. Then, we break down the effective mix fraction into its various constituents based on their most likely sources. In Sec. III, we discuss the impact of the observed mix on target performance. Finally, in Sec. IV, we discuss the results and implications for current and future work.

II. EXPERIMENTAL ANALYSIS

In order to effectively mitigate the deleterious impact of mix, we desire to quantify how much mix is present in our

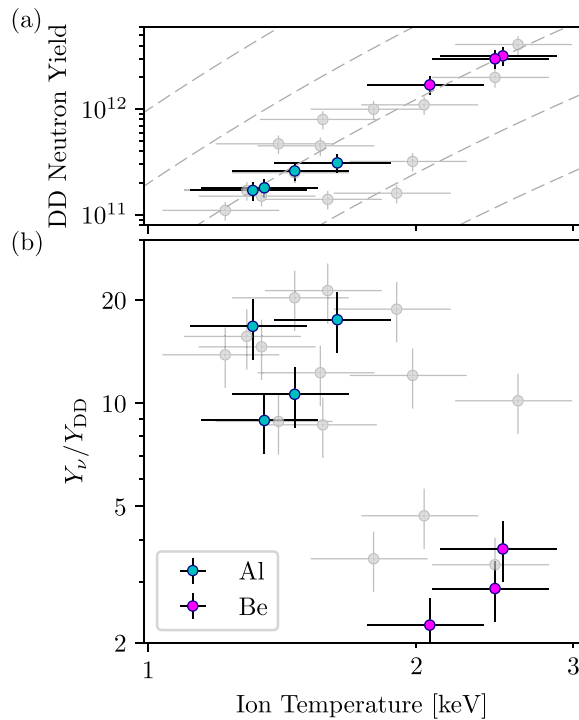


FIG. 2. (a) Plot of measured DD neutron yield vs. ion temperature inferred using neutron time of flight detectors. Cyan points are those experiments that had Al cushions, and magenta points are those that had Be cushions. Grey points are other experiments for reference. The dashed grey lines are proportional to the DD fusion reactivity. (b) Plot of x-ray to neutron yield ratio vs. ion temperature.

experiments and to understand its origins. To this end, the suite of experiments were analyzed to determine the average stagnation pressure and the effective mix fraction, defined as the equivalent mix fraction assuming that all the mix is Be. The effective mix fraction determined in this way is only sensitive to how much mix is present during burn and thus does not by itself

TABLE I. Table summarizing the configuration and performance of the experiments discussed in this paper. Each shot is identified by its shot number and the cushion material. The preheat energy (E_{PH}) is split into the energy output by ZBL in the pre-pulse and the main pulse. The DD neutron yield (Y_{DD}) is measured using activation detectors. The x-ray yield (Y_ν) is measured using filtered PCDs. The ion temperature (T_i) is measured by using the neutron time of flight detectors. The hotspot volume (V_{HS}) is measured using a time integrated, monochromatic x-ray imaging system. The fuel pressure (P_{HS}) and effective mix fraction (f_{eff}) are described in the text.

Z Shot #	Cushion material	E_{PH} [kJ]	$Y_{DD} (\pm 20\%) \times 10^{12}$	Y_ν [J]	T_i [keV]	V_{HS} [cm ³]	P_{HS} [Gbar]	f_{eff} [%]
z2707	Al	0.3 + 1.8	0.3	3.1	1.5	0.8×10^{-4}	0.51	16.3
z2708	Al	0.4 + 2.3	0.2	3.2	1.3	1.1×10^{-4}	0.55	21.2
z2758	Al	0.4 + 1.8	0.3	6.1	1.6	1.0×10^{-4}	0.59	21.0
z2985	Al	0.6 + 2.1	0.2	1.8	1.4	0.8×10^{-4}	0.54	17.0
z2839	Be	0.4 + 2.3	3.2	13.5	2.3	1.2×10^{-4}	0.78	7.3
z2977	Be	0.4 + 2	3.0	9.7	2.5	0.9×10^{-4}	0.75	5.8
z2979	Be	0.3 + 1.8	1.7	4.3	2.2	1.0×10^{-4}	0.68	4.9

elucidate the origins and timing of the various mix sources. Simulations of uniform fuel mix indicate that yield degradation worsens with increasing mix fractions, atomic number, and duration. In other words, MagLIF performance is much more sensitive to mix introduced during the preheat stage than it is to mix introduced near stagnation.⁶

In Z experiments, the ion temperature, stagnation volume, and burn time are measured using neutron time of flight detectors, self-emission imaging, and x-ray power detectors, respectively. Examples of typical self-emission images obtained using a spherical crystal imager are shown in Fig. 3, where (a) and (b) correspond to Al cushion experiments and (c) and (d) correspond to Be cushion experiments. The imagers were configured slightly differently in each case, accounting for the different noise levels on each experiment. Additionally, on shot z2839, there was a strip of plastic used to block a portion of the emission to create a spatial fiducial for alignment purposes [area between the dashed lines in Fig. 3(c)]. Although there are shot to shot variations, we do not see obvious qualitative differences in the morphology of the stagnation columns in these images, with each exhibiting the helical structure characteristic of these magnetized implosions.^{17,18} Further analysis reveals similar average radii and total column lengths in each case ($< \pm 10\%$), indicating that the compressional work done on the fuel is approximately the same. We define a volume using the contour enclosing 85% of the emission and assume that each axial position is cylindrically symmetric (see Table I).

The above hotspot metrics can be incorporated with a model for the x-ray and neutron emission to infer the pressure and mix fraction. We write the energy dependent radiation power following Ma et al.¹⁵ and Epstein et al.¹⁹ as

$$P_\nu = 4\pi e^{-\tau_\nu} \int_{V_{HS}} \langle Z \rangle g_{FF} \sum_i f_i j_i dV. \quad (1)$$

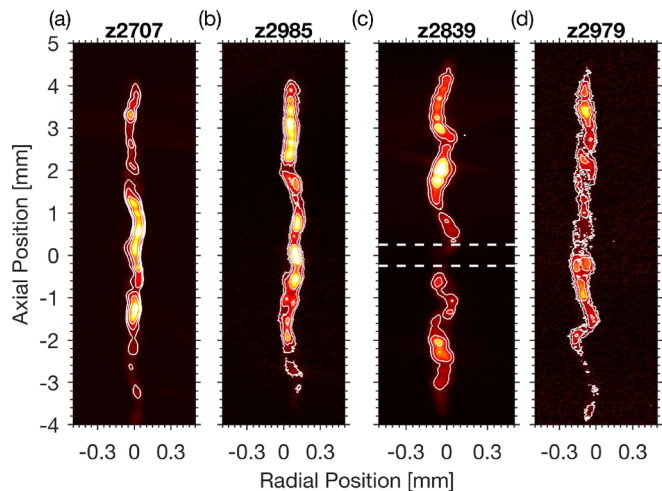


FIG. 3. Spherical crystal image from z2707 (a) and z2985 (b), Al cushion experiments, and z2839 (c) and z2979 (d), Be cushion experiments. White contours indicate the 10%, 20%, and 40% intensity levels. The dim region denoted by the dashed white lines in (c) is caused by a fiducial placed in the path of the image.

Here, the integral is over the fuel volume, τ_ν^ℓ is the liner opacity, g_{FF} is the free-free gaunt factor,¹⁹ $\langle Z \rangle$ is the average charge state of the fuel, and f_i and j_i are the fraction and emissivity of each species in the fuel, respectively. The emissivity is the sum of the free-free and free-bound contributions, which can be expressed as

$$j_i^{ff} = A_{ff} \frac{n_i^2 Z_i^2}{T_e^{1/2}} e^{-h\nu/T_e}, \quad (2)$$

$$j_i^{fb} = A_{fb} \frac{n_i^2 Z_i^4}{T_e^{3/2}} e^{Ry Z_i^2/T_e} e^{-h\nu/T_e}, \quad (3)$$

where $A_{ff} = 2 \times 10^{-32} \text{ W cm}^3 \text{ eV}^{-1/2}$ is the free-free emission coefficient, $A_{fb} = 4 \times 10^{-31} \text{ W cm}^3 \text{ eV}^{1/2}$ is the free-bound emission coefficient, $Ry = 13.6 \text{ eV}$ is the Rydberg constant, and T_e is the plasma electron temperature. Using an ideal-gas equation of state and assuming an isobaric hotspot, we replace the fuel density in favor of the pressure P_{HS} , which is then removed from the volume integral. This gives

$$P_\nu = A_{ff} 4\pi P_{HS}^2 e^{-\tau_\nu^\ell} \int_{V_{HS}} \frac{\langle Z \rangle g_{FF}}{(1 + \langle Z \rangle)^2} \sum_i f_i j_i \frac{e^{-h\nu/T_e}}{T_e^{5/2}} dV, \quad (4)$$

where $\tilde{j}_i \equiv j_i/j_D = Z_i^2 + (A_{fb}/A_{ff})(Z_i^4/T_e) e^{Ry Z_i^2/T_e}$. The total x-ray emission is obtained by multiplying Eq. (4) by the spectral response of the Photoconducting Diamond (PCD) detector and filters used in the experiment and integrating over time and photon energy.

Following the same method, the neutron emission is described by the following expression:

$$Y_{DD} = \frac{1}{2} P_{HS}^2 \tau_b \int_{V_{HS}} \frac{\langle \sigma v \rangle_{DD}}{(1 + \langle Z \rangle)^2 T_i^2} dV, \quad (5)$$

where τ_b is the burn duration (measured using x-rays) and $\langle \sigma v \rangle_{DD}$ is the DD fusion reactivity.²⁰ By assuming that the ion and electron temperatures are equal and assuming a radial temperature dependence as described by McBride and Slutz,¹² we can determine the stagnation pressure and mix fraction that best fits the observed neutron and x-ray emission, given the measurements of T_i , volume, and burn duration as inputs. The

results of this analysis are shown in Fig. 4 and are tabulated in the final two columns of Table I as P_{HS} and f_{eff} .

There is a clear distinction between these two classes of experiments, where a high effective mix fraction is correlated with a lower stagnation pressure. Furthermore, we can calculate the internal energy of the fuel at stagnation assuming $E_f = \frac{3}{2} P_{HS} V_{HS}$. The Al cushion experiments have $E_f \approx 7.6 \text{ kJ}$, while the Be cushion experiments have $E_f \approx 11.4 \text{ kJ}$, an $\sim 50\%$ increase in fuel energy.

Because each experiment used the same target geometry, laser pulse shape, current drive, and LEH window, we can approximately reconstruct the quantities of mix from the various potential sources. Following Slutz et al.,⁶ we assume that the radiative losses are proportional to Z^3 . Additionally, we consider three main sources of mix for our experiments: the LEH window, the top cushion, and the deceleration-phase liner mix. With these considerations, we obtain the following relations:

$$f_{eff}^{Be} Z_{Be}^3 = f_W \bar{Z}_{poly}^3 + f_C^{Be} Z_{Be}^3 + f_D Z_{Be}^3, \quad (6)$$

$$f_{eff}^{Al} Z_{Be}^3 = f_W \bar{Z}_{poly}^3 + f_C^{Al} Z_{Al}^3 + f_D Z_{Be}^3. \quad (7)$$

Let us comment on the terms appearing in the equations above. The effective mix fraction $f_{eff}^{Be/Al}$ is the mix fraction obtained when assuming fully ionized Be and represents the total mix from all sources present at stagnation. Here, the superscripts denote the effective mix fractions for the experiments with Be cushions and Al cushions, respectively. Note that $f_{eff}^{Be/Al}$ is obtained by using Eqs. (4)–(5) together with the experimental measurements for the ion temperature T_i , x-ray yield Y_ν , and DD neutron yield Y_{DD} .

The first terms on the right-hand side of Eqs. (6) and (7) represent the mix introduced by the window. The window mix is assumed to originate prior to stagnation due to the laser heating and is composed of fully ionized polyimide $C_{22}H_{10}N_2O_5$, which results in an average ionization of $\bar{Z}_{poly} = 6$ for each of the 39 ions per molecule when a Z^3 weighting is used. We can approximate the amount of window material injected into the fuel by considering the initial geometry of the window and the laser spot size. Assuming a square spot size of 0.5 mm and using the initial thickness of the window ($1.77 \mu\text{m}$), we find that $\sim 10^{15}$ window molecules are mixed into the fuel, resulting in $\sim 4 \times 10^{16}$ ions. Using the inferred stagnation pressure and the measured volume and temperature, we can estimate the number of fuel ions participating in stagnation ($\sim 8 \times 10^{18}$), giving a window mix fraction of $f_W \approx 0.5\%$.

Regarding the second and last terms on the right-hand side of Eqs. (6) and (7), $f_C^{Be/Al}$ denotes the mix fraction introduced by the Be or Al cushions, respectively. Similarly, as for the window mix, cushion mix originates prior to stagnation due to the laser heating. Upon assuming that the same mass of cushion material is ablated into the fuel during the preheat stage, one can relate the Be and Al cushion mix fractions: $f_C^{Al} = \frac{1}{3} f_C^{Be}$. Finally, the last terms in Eqs. (6) and (7) represent the deceleration phase mix introduced into the fuel at or near stagnation as the heavy liner decelerates on the hot fuel. This mix is mainly composed of Be. For our analysis, we assume that all sources of mix are uniformly distributed in the hotspot by stagnation when our observations occur.

With the above considerations, Eqs. (6) and (7) are fully determined. Solving the equations leads to a Be cushion mix

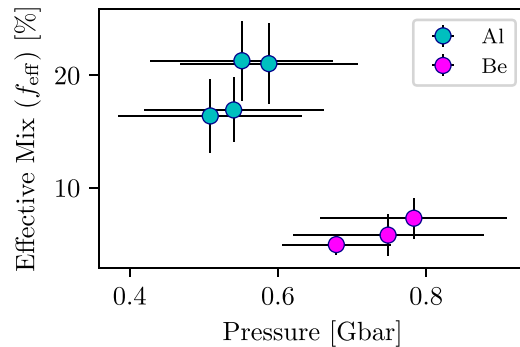


FIG. 4. Volume averaged hotspot pressure vs. effective mix fraction.

fraction of $f_C^{\text{Be}} = 1.7\%$, an Al cushion mix fraction of $f_C^{\text{Al}} = 0.58\%$, and a deceleration mix fraction of $f_D = 2.4\%$. These cushion and liner mix fractions correspond to a layer of Be of only ~ 90 nm and ~ 15 nm, respectively. The analysis above hinges on several assumptions, which could potentially be violated. First, we assumed that the mass of Al is equal to the mass of Be ablated from the cushions. This assumption was motivated by a desire to conserve the kinetic energy of the ablated material. It is worth mentioning that we could have assumed that the same volume of material is ablated from the cushions so that $f_C^{\text{Al}} = \frac{1}{2}f_C^{\text{Be}}$. Second, in our analysis, we determined the window mix fraction by considering all the plastic molecules contained within the laser spot. It is a possibility that this is a conservative estimate, as laser heating experiments with the unconditioned beam show that the blast wave is much larger than the laser spot size, implying that the laser could be interacting over a larger area.¹¹ Alternatively, one might expect that some of the window material is ablated out of the fuel, making the previous assumption pessimistic. To assess this, we varied by $\pm 50\%$ the number of window ions mixed in. Taken together, these variations imply $f_W \simeq 0.5 \pm 0.2\%$, $f_C^{\text{Be}} = 1.45 \pm 0.3\%$, $f_C^{\text{Al}} = 0.57 \pm 0.05\%$, and $f_D = 2.6 \pm 0.6\%$.

III. EFFECT OF MIX ON PERFORMANCE

It is apparent from this analysis that just under half of the mix present during burn is sourced from non-imploding portions of the target, namely, the window and the cushion. Mix from these sources must be introduced prior to stagnation as the rising pressure during the implosion would tend to otherwise force material from these components outward. In light of these results, we now believe that the laser heating phase is responsible for the generation and subsequent transport of this material into the fuel. In fact, data from experiments where coatings were placed on the window or the top cushion show x-ray line emission in the upper portion of the stagnation column, proving the presence of mix from these components during burn.³ This study puts constraints on how much material is present, the accuracy of which would be improved if the components of interest could be volumetrically doped, instead of coated.

Because the window is solid density plastic, a substantial fraction of the laser energy ($\sim 50\%$) is invested into disassembling the window. Additionally, the upper portion of the gas must be heated first before the laser can penetrate deeper into the column. Both of these effects lead to the production of a blast wave in the region underneath the window, which has a net flow both radially outward and axially downward. This process could entrain window and cushion material in the flow, mixing it into the fuel. Furthermore, as the blast wave exits the bottom of the cushion and expands into the larger cavity defined by the liner wall, it can scrape the material from the cushion and transport it into the fuel region. Additionally, the laser configuration used in these experiments is strongly susceptible to laser plasma instabilities,¹¹ such as strong filamentation and scattering. This could cause direct ablation of the material from the cushion, which would then be transported into the fuel by the blast wave. Since the cushion is a smaller diameter than the

liner, it acts as a sort of collimator for these effects. Therefore, even though we expect that the laser could directly interact with the cushion, it is unlikely to do so with the liner itself.

It is worth mentioning that the above inferred mix fractions imply much more yield degradation than observed if they are present and uniformly distributed at the time of preheat. Figure 5(a) from the study by Slutz *et al.* shows the yield degradation from a series of 1D calculations with various mix fractions of different elements.⁶ Looking at the case of 1.5% Be, we see approximately $\sim 5\times$ degradation compared to the clean case. Alternatively, for 0.5% Al, the 1D calculations predict $\gg 100\times$ degradation, which is inconsistent with the observation of a factor of $10\times$ between the Be and Al cushion cases. This suggests several possibilities. First, although the mix is generated during the laser heating phase, it is not widely distributed until later, when it becomes more thoroughly mixed. Second, the material may never become fully mixed and may be more heterogeneously distributed. In fact, the spectroscopic evidence reported in Ref. 3 shows that window mix is confined to the upper ~ 3 mm of the stagnation column. This observation logically extends to the cushion mix as well.

Nevertheless, we can ask the question: what yield might we expect according to the existing observations if the cushions were coated with a layer of D_2 ice? This case represents the least detrimental element that could be mixed into the fuel. Although the measured yield degradation as a function of the impurity fraction does not correspond to the values reported in Ref. 6, we assume that the trend is reasonable. We find that the calculated yield degradation is well approximated as an exponential, giving

$$\frac{Y_i}{Y_{\text{Be}}} = A \exp(-\alpha x_i). \quad (8)$$

Here, $x_i = (f_i Z_i^3)/(f_{\text{Be}} Z_{\text{Be}}^3)$ is the Z-weighted mix fraction relative to that of Be, assumed to be our baseline case. Using this model for yield degradation, we extrapolate to the performance of a deuterium “mixed” target for each of the assumed cases in Sec. II (i.e., cushion mix mass or volume is conserved when the material changes).

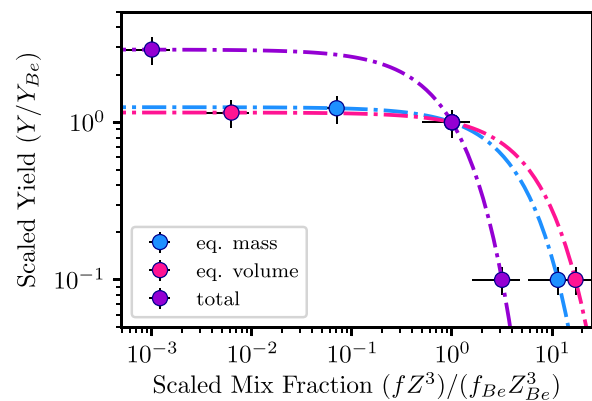


FIG. 5. Yield degradation results by assuming equal mixed mass from cushions (blue), equal mixed volume from cushions (pink), and total effective mix fraction (purple). For the total effective mix case, $x_D = 1 \times 10^{-3}$ instead of 0 to be visible on a log scale.

First, we determine the x_i for the assumption of conserved mix mass and conserved mix volume. In both cases, $x_{\text{Be}} \equiv 1$ by construction. $Y_{\text{Al}}/Y_{\text{Be}} = 0.1$, and we find that $x_{\text{Al}} \approx 11$ when we assume equal masses of Be and Al cushion mix and $x_{\text{Al}} \approx 17$ when we assume that equal volumes of material are mixed. Replacing the mixed material with deuterium gives $x_{\text{D}} = 0.07$ and $x_{\text{D}} = 0.006$ for equal mass and equal volume, respectively. Plugging this information into Eq. (8), we find that $Y_{\text{D}}/Y_{\text{Be}} = 1.15 - 1.25$. This says that mitigating the cushion mix alone provides only an $\sim 20\%$ improvement compared to the Be cushion case. This also implies that the change from Al to Be cushions has already nearly maximized our expected performance gains from mitigating cushion mix.

Alternatively, we can use the effective total mix fractions determined in Sec. II ($f_{\text{eff}}^{\text{Be}} \approx 6\%$ and $f_{\text{eff}}^{\text{Al}} \approx 19\%$) and ask what the yield would be if we removed all sources of mix. This estimate attempts to account for the degradation caused by all of the sources of mix, not just that of the cushion. In this scenario, $x_{\text{Be}} = 1$, $x_{\text{Al}} = 3.1$, and $x_{\text{D}} = 0$. This results in a more substantial improvement of $2.9\times$ over the Be cushion case. These results are summarized in Fig. 5. This analysis is likely to be an upper bound to the potential improvement, as it uses as its basis a model that assumes uniform mix at the time of preheat and as stated we see evidence in the data that the window and liner mix are not uniformly distributed.

IV. CONCLUSIONS

We have conclusively demonstrated that mix from the cushions in MagLIF experiments can dramatically degrade target performance and that reducing the atomic number of this source of impurities significantly improves performance. In the series of experiments discussed, changing the cushions from Al to Be resulted in a $10\times$ increase in neutron yield, an $\sim 50\%$ increase in the hotspot energy, and an $\sim 60\%$ increase in the measured ion temperature. Further analysis of these experiments revealed that at stagnation, in the higher performing case, the hotspot is composed approximately of $\sim 0.5\%$ window material, $\sim 1.5\%$ Be cushion material, and $\sim 2.6\%$ liner material. Before these observations, it was not expected that the cushions or window would be a significant source of mix, but these components are shown to account for almost half of the observed mix at stagnation, the remainder likely coming from the liner.

It is shown based on extrapolation of the available data using a model motivated by detailed physics calculations that the remaining Be cushion mix is likely a small perturbation on the target performance. Attempting to account for the total mix observed in the targets shows that, in the experimental configuration presented here, there may be a factor of $\sim 2.9\times$ in yield to be gained by eliminating mix entirely, which is likely an upper bound.

These results lead to the exclusive use of Be fuel-facing components in subsequent MagLIF experiments. Additionally, significant effort has gone into optimizing the laser heating protocol to simultaneously minimize window mix and increase the energy deposited into the fuel,^{3,11} resulting in enhanced performance. The results shown here represent a volume averaged analysis. However, the stagnation parameters and distribution of

mix are unlikely to be uniform. Future work will be focused on understanding these spatial variations to elucidate the impact of non-uniform mix and the role of the stagnation morphology in determining performance.

ACKNOWLEDGMENTS

Sandia National Laboratories is a multimission laboratory managed and operated by the National Technology & Engineering Solutions of Sandia, LLC, a wholly owned subsidiary of Honeywell International, Inc., for the U.S. Department of Energy's National Nuclear Security Administration under Contract No. DE-NA0003525. This paper describes objective technical results and analysis. Any subjective views or opinions that might be expressed in the paper do not necessarily represent the views of the U.S. Department of Energy or the U.S. Government. Portions of this work were supported by the U.S. Department of Energy under Contract Nos. DE-SC0016252 and DE-NA0001944 and NSF Grant No. PHY-1725178.

REFERENCES

- ¹S. A. Slutz, M. C. Herrmann, R. A. Vesey, A. B. Sefkow, D. B. Sinars, D. C. Rovang, K. J. Peterson, and M. E. Cuneo, *Phys. Plasmas* **17**, 056303 (2010).
- ²M. R. Gomez, S. A. Slutz, A. B. Sefkow, D. B. Sinars, K. D. Hahn, S. B. Hansen, E. C. Harding, P. F. Knapp, P. F. Schmit, C. A. Jennings, T. J. Awe, M. Geissel, D. C. Rovang, G. A. Chandler, G. W. Cooper, M. E. Cuneo, A. J. Harvey-Thompson, M. C. Herrmann, M. H. Hess, O. Johns, D. C. Lamppa, M. R. Martin, R. D. McBride, K. J. Peterson, J. L. Porter, G. K. Robertson, G. A. Rochau, C. L. Ruiz, M. E. Savage, I. C. Smith, W. A. Stygar, and R. A. Vesey, *Phys. Rev. Lett.* **113**, 155003 (2014).
- ³A. J. Harvey-Thompson, A. B. Sefkow, T. N. Nagayama, M. S. Wei, E. M. Campbell, G. Fiksel, P.-Y. Chang, J. R. Davies, D. H. Barnak, V. Y. Glebov, P. Fitzsimmons, J. Fooks, and B. E. Blue, *Phys. Plasmas* **22**, 122708 (2015).
- ⁴P. F. Schmit, P. F. Knapp, S. B. Hansen, M. R. Gomez, K. D. Hahn, D. B. Sinars, K. J. Peterson, S. A. Slutz, A. B. Sefkow, T. J. Awe, E. Harding, C. A. Jennings, G. A. Chandler, G. W. Cooper, M. E. Cuneo, M. Geissel, A. J. Harvey-Thompson, M. C. Herrmann, M. H. Hess, O. Johns, D. C. Lamppa, M. R. Martin, R. D. McBride, J. L. Porter, G. K. Robertson, G. A. Rochau, D. C. Rovang, C. L. Ruiz, M. E. Savage, I. C. Smith, W. A. Stygar, and R. A. Vesey, *Phys. Rev. Lett.* **113**, 155004 (2014).
- ⁵P. F. Knapp, P. F. Schmit, S. B. Hansen, M. R. Gomez, K. D. Hahn, D. B. Sinars, K. J. Peterson, S. A. Slutz, A. B. Sefkow, T. J. Awe, E. Harding, C. A. Jennings, M. P. Desjarlais, G. A. Chandler, G. W. Cooper, M. E. Cuneo, M. Geissel, A. J. Harvey-Thompson, J. L. Porter, G. A. Rochau, D. C. Rovang, C. L. Ruiz, M. E. Savage, I. C. Smith, W. A. Stygar, and M. C. Herrmann, *Phys. Plasmas* **22**, 056312 (2015).
- ⁶S. A. Slutz, M. R. Gomez, S. B. Hansen, E. C. Harding, B. T. Hutsel, P. F. Knapp, D. C. Lamppa, T. J. Awe, D. J. Ampleford, D. E. Bliss, G. A. Chandler, M. E. Cuneo, M. Geissel, M. E. Glinsky, A. J. Harvey-Thompson, M. H. Hess, C. A. Jennings, B. Jones, G. R. Laity, M. R. Martin, K. J. Peterson, J. L. Porter, P. K. Rambo, G. A. Rochau, C. L. Ruiz, M. E. Savage, J. Schwarz, P. F. Schmit, G. Shipley, D. B. Sinars, I. C. Smith, R. A. Vesey, and M. R. Weis, *Phys. Plasmas* **25**, 112706 (2018).
- ⁷P. K. Rambo, I. C. Smith, J. L. Porter, Jr., M. J. Hurst, C. S. Speas, R. G. Adams, A. J. Garcia, E. Dawson, B. D. Thurston, C. Wakefield, J. W. Kellogg, M. J. Slattery, H. C. Ives III, R. S. Broyles, J. A. Caird, A. C. Erlandson, J. E. Murray, W. C. Behrendt, N. D. Neilsen, and J. M. Narduzzi, *Appl. Opt.* **44**, 2421 (2005).
- ⁸P. Rambo, J. Schwarz, M. Schollmeier, M. Geissel, I. Smith, M. Kimmel, C. Speas, J. Shores, D. Armstrong, J. Bellum, E. Field, D. Kletecka, and J. Porter, "Sandia's z-backlighter laser facility," *Proc. SPIE* **10014**, 100140Z (2016).

- ⁹M. Savage, K. LeChien, W. Stygar, J. Maenchen, D. McDaniel, and K. Struve, in *Proceedings of the IEEE International Power Modulators and High Voltage Conference* (2008), pp. 93–93.
- ¹⁰D. C. Rovang, D. C. Lamppa, M. E. Cuneo, A. C. Owen, J. McKenney, D. W. Johnson, S. Radovich, R. J. Kaye, R. D. McBride, C. S. Alexander, T. J. Awe, S. A. Slutz, A. B. Sefkow, T. A. Haill, P. A. Jones, J. W. Argo, D. G. Dalton, G. K. Robertson, E. M. Waisman, D. B. Sinars, J. Meissner, M. Milhous, D. N. Nguyen, and C. H. Mielke, *Rev. Sci. Instrum.* **85**, 124701 (2014).
- ¹¹M. Geissel, A. J. Harvey-Thompson, T. J. Awe, D. E. Bliss, M. E. Glinsky, M. R. Gomez, E. Harding, S. B. Hansen, C. Jennings, M. W. Kimmel, P. Knapp, S. M. Lewis, K. Peterson, M. Schollmeier, J. Schwarz, J. E. Shores, S. A. Slutz, D. B. Sinars, I. C. Smith, C. S. Speas, R. A. Vesey, M. R. Weis, and J. L. Porter, *Phys. Plasmas* **25**, 022706 (2018).
- ¹²R. D. McBride and S. A. Slutz, *Phys. Plasmas* **22**, 052708 (2015).
- ¹³R. D. McBride, S. A. Slutz, R. A. Vesey, M. R. Gomez, A. B. Sefkow, S. B. Hansen, P. F. Knapp, P. F. Schmit, M. Geissel, A. J. Harvey-Thompson, C. A. Jennings, E. C. Harding, T. J. Awe, D. C. Rovang, K. D. Hahn, M. R. Martin, K. R. Cochrane, K. J. Peterson, G. A. Rochau, J. L. Porter, W. A. Stygar, E. M. Campbell, C. W. Nakhleh, M. C. Herrmann, M. E. Cuneo, and D. B. Sinars, *Phys. Plasmas* **23**, 012705 (2016).
- ¹⁴K. D. Hahn, G. A. Chandler, C. L. Ruiz, G. W. Cooper, M. R. Gomez, S. Slutz, A. B. Sefkow, D. B. Sinars, S. B. Hansen, P. F. Knapp, P. F. Schmit, E. Harding, C. A. Jennings, T. J. Awe, M. Geissel, D. C. Rovang, J. A. Torres, J. A. Bur, M. E. Cuneo, V. Y. Glebov, A. J. Harvey-Thompson, M. C. Herrman, M. H. Hess, O. Johns, B. Jones, D. C. Lamppa, J. S. Lash, M. R. Martin, R. D. McBride, K. J. Peterson, J. L. Porter, J. Reneker, G. K. Robertson, G. A. Rochau, M. E. Savage, I. C. Smith, J. D. Styron, and R. A. Vesey, *J. Phys.: Conf. Ser.* **717**, 012020 (2016).
- ¹⁵T. Ma, P. K. Patel, N. Izumi, P. T. Springer, M. H. Key, L. J. Atherton, L. R. Benedetti, D. K. Bradley, D. A. Callahan, P. M. Celliers, C. J. Cerjan, D. S. Clark, E. L. Dewald, S. N. Dixit, T. Döppner, D. H. Edgell, R. Epstein, S. Glenn, G. Grim, S. W. Haan, B. A. Hammel, D. Hicks, W. W. Hsing, O. S. Jones, S. F. Khan, J. D. Kilkenny, J. L. Kline, G. A. Kyrala, O. L. Landen, S. Le Pape, B. J. MacGowan, A. J. Mackinnon, A. G. MacPhee, N. B. Meezan, J. D. Moody, A. Pak, T. Parham, H.-S. Park, J. E. Ralph, S. P. Regan, B. A. Remington, H. F. Robey, J. S. Ross, B. K. Spears, V. Smalyuk, L. J. Suter, R. Tommasini, R. P. Town, S. V. Weber, J. D. Lindl, M. J. Edwards, S. H. Glenzer, and E. I. Moses, *Phys. Rev. Lett.* **111**, 085004 (2013).
- ¹⁶R. D. McBride, M. R. Martin, R. W. Lemke, J. B. Greenly, C. A. Jennings, D. C. Rovang, D. B. Sinars, M. E. Cuneo, M. C. Herrmann, S. A. Slutz, C. W. Nakhleh, D. D. Ryutov, J.-P. Davis, D. G. Flicker, B. E. Blue, K. Tomlinson, D. Schroen, R. M. Stamm, G. E. Smith, J. K. Moore, T. J. Rogers, G. K. Robertson, R. J. Kamm, I. C. Smith, M. Savage, W. A. Stygar, G. A. Rochau, M. Jones, M. R. Lopez, J. L. Porter, and M. K. Matzen, *Phys. Plasmas* **20**, 056309 (2013).
- ¹⁷T. J. Awe, R. D. McBride, C. A. Jennings, D. C. Lamppa, M. R. Martin, D. C. Rovang, S. A. Slutz, M. E. Cuneo, A. C. Owen, D. B. Sinars, K. Tomlinson, M. R. Gomez, S. B. Hansen, M. C. Herrmann, J. L. McKenney, C. Nakhleh, G. K. Robertson, G. A. Rochau, M. E. Savage, D. G. Schroen, and W. A. Stygar, *Phys. Rev. Lett.* **111**, 235005 (2013).
- ¹⁸T. J. Awe, C. A. Jennings, R. D. McBride, M. E. Cuneo, D. C. Lamppa, M. R. Martin, D. C. Rovang, D. B. Sinars, S. A. Slutz, A. C. Owen, K. Tomlinson, M. R. Gomez, S. B. Hansen, M. C. Herrmann, M. C. Jones, J. L. McKenney, G. K. Robertson, G. A. Rochau, M. E. Savage, D. G. Schroen, and W. A. Stygar, *Phys. Plasmas* **21**, 056303 (2014).
- ¹⁹R. Epstein, V. N. Goncharov, F. J. Marshall, R. Betti, R. Nora, A. R. Christopherson, I. E. Golovkin, and J. J. MacFarlane, *Phys. Plasmas* **22**, 022707 (2015).
- ²⁰H.-S. Bosch and G. M. Hale, *Nucl. Fusion* **32**, 611 (1992).